

---

# Remote Sensing Change Detection (Segmentation) using Denoising Diffusion Probabilistic Models

---

Wele Gedara Chaminda Bandara, Nithin Gopalakrishnan Nair, Vishal M. Patel

Johns Hopkins University, USA.

wbandar1@jhu.edu, ngopala2@jhu.edu, vpatel36@jhu.edu

Project page: <https://github.com/wgcbn/ddpm-cd>

## Abstract

Human civilization has an increasingly powerful influence on the earth system, and earth observations are an invaluable tool for assessing and mitigating the negative impacts. To this end, observing precisely defined changes on Earth’s surface is essential, and we propose an effective way to achieve this goal. Notably, our change detection (CD)/ segmentation method proposes a novel way to incorporate the millions of off-the-shelf, unlabeled, remote sensing images available through different earth observation programs into the training process through denoising diffusion probabilistic models. We first leverage the information from these off-the-shelf, uncurated, and unlabeled remote sensing images by using a pre-trained denoising diffusion probabilistic model and then employ the multi-scale feature representations from the diffusion model decoder to train a lightweight CD classifier to detect precise changes. The experiments performed on four publically available CD datasets show that the proposed approach achieves remarkably better results than the state-of-the-art methods in F1, IoU and overall accuracy. Code and pre-trained models are available at: <https://github.com/wgcbn/ddpm-cd>



Figure 1: Images generated from the diffusion model trained on off-the-shelf remote sensing images. The generated images contain objects that we commonly see in real remote sensing images, such as buildings, trees, roads, vegetation, water surfaces, etc., demonstrating the powerful ability of the diffusion models to extract key semantics that can be further used in remote sensing change detection.

## 1 Introduction

The results of a recent poll published in The Washington Post shows that people around the world are increasingly concerned about climate change and are aware of human activities related to global climate than ever before. With global climate measures such as atmospheric carbon dioxide concentration, global average surface temperature, and sea level rise, it is now possible to observe changes at global scale due to climate change. On the other hand, accurate predictions of local land cover changes such as changes due to deforestation, floods, forest fires, urbanization, and use of land for agriculture are also of critical importance as an essential climate variable [5] and for climate change mitigation programs such as UN-REDD+.

Thanks to various satellite programs of the National Aeronautics and Space Administration (NASA), the European Space Agency (ESA), the United States Geological Survey (USGS), and many other government/private entities around the world, we now witness more than 24 million publicly available satellite images from the last 37 years as of 2021, making remote sensing images as the effective and reliable data source for monitoring local changes in the Earth's surface.

Even though we have access to millions of remote sensing images to monitor local changes, predicting changes of interest is a challenging task to tackle through computer vision due to the fact that the high diversity of data, seasonal variations of Earth's surface, different levels of solar illumination, different imaging styles and sensors, spectral variability, etc [49, 48]. In addition, annotating changes in remote sensing images requires comparison of two or more images in the time series data by the human experts, which is indeed a time consuming and expensive process, making the available CD datasets to have less annotated training images (mostly around a couple thousand images) available to train the CD model.

Therefore, an effective and robust CD model should not only focus on exploiting the information from limited annotated data available for training the model, but also focus on exploiting as much information as possible from millions of freely available, unlabeled and uncurated remote sensing images to improve the accuracy and robustness of the CD. How to effectively harness the information from these large collections of uncurated remote sensing images is a long-standing question, and much effort has been devoted to answering this question in the past.

Remote sensing pre-training [47] is one of the most widely adopted techniques for this purpose. With the emergence of large-scale areal-scene recognition datasets such as MillionAID [28], fMoW [12] and BigEarthNet [45], one can pre-train the encoder of the CD model to capture the key feature representations (i.e., semantics) of remote sensing images. However, the need for image-level class labels hinders its ability to train on millions of unlabeled and uncurated remote sensing images, which has motivated the researchers to explore self-supervised pre-training methods [10, 11, 52] such as SeCo [31], where the presence of seasonal changes in aerial scenes is used to ensure consistency between positive samples.

Different from the above pre-training techniques, in this paper, we show that the diffusion probabilistic models [42, 20, 33] can also be used to extract key semantics of remote sensing images. Diffusion models are directed graphical models parameterized by a Markov chain (see figure 2). We train a diffusion model using a variational inference procedure on a large collection of off-the-shelf remote sensing images to generate images that are closer to real images over the finite time. Figure 1 shows some sample images generated from the diffusion model. We can see that the generated images are very closer to the actual remote sensing images and contains key objects find in remote sensing images, such as buildings, trees, vegetation, roads, water surfaces, etc. Therefore, diffusion model is powerful enough to extract key features of a given image. While any generative model (such as VAEs [23, 24]

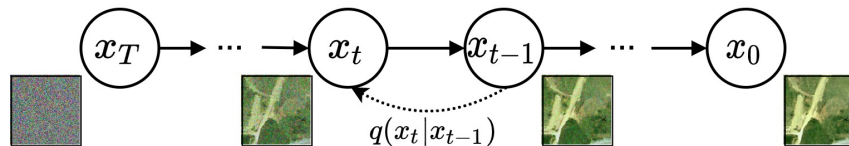


Figure 2: The diffusion model as a directed graphical model [20].

or GANs [18, 44]) can be trained to learn key semantics in a similar way, based on our experiments, diffusion models have been shown to produce better feature representations. From the experiments, we observe that the representational power of VAE and GANs are limited compared to diffusion models, resulting in lower CD performance (see the supplementary material for more details). Since diffusion models can be used to extract better semantics of given a image, we fine-tune a light-weight CD classifier with the limited pixel-level change labels by utilizing multi-scale semantics (i.e., deep feature representations) from the diffusion model as its inputs. Experiments conducted on multiple CD datasets show that the proposed method achieves significant performance improvement over the state-of-the-art (SOTA) CD methods, demonstrating that diffusion probabilistic models can be used not only to sample images closer to the training data distribution, but also to extract deep semantics that are useful for low-level vision tasks.

## 2 Background

### 2.1 Diffusion Models

Diffusion probabilistic models [20, 42, 41, 32, 37] belong to the class of generative models where, once trained, we can use the model to generate high-quality images that are closer to the training data distribution. Unlike other generative models such as Generative Adversarial Networks (GANs), Variational Autoencoders (VAEs), autoregressive models and flows, diffusion models are efficient to train and have been widely adopted in several applications, including super-resolution [41], deblurring [50], segmentation [51, 22, 4], image colorization [43], inpainting [43], and semantic editing [38]. However, there is still no demonstration of the application of diffusion models in remote sensing applications despite its high potential and great success in other machine vision applications. In this work, we demonstrate that remote sensing CD can also benefit from diffusion models, opening a new direction to explore remote sensing applications in the future. In the following sections, we provide a brief overview of the diffusion framework.

**Gaussian Diffusion Process.** Diffusion models learn the training data distribution  $p(x_0)$  by performing variational inference on a Markovian process with  $T$  number of timesteps. The diffusion process consists of a forward process as well as a backward process. In the forward process, we gradually add Gaussian noise to the clean image  $x_0 \sim p(x_0)$  until the image is completely destroyed resulting in an isotropic gaussian distribution  $\mathcal{N}(\mathbf{0}, \mathbf{I})$ . The noising operation at each time step  $t$  in the forward process is defined as follows:

$$q(x_t|x_{t-1}) = \mathcal{N}(x_t; \sqrt{\alpha_t}x_{t-1}, (1 - \alpha_t)\mathbf{I}), \quad (1)$$

where  $(x_0, x_1, \dots, x_T)$  denotes the  $T$ -step Markov chain (see Fig. 2),  $\alpha_{1:T} = (\alpha_1, \dots, \alpha_T)$  is the noise schedule that controls the variance of noise added at each step. In the reverse process a sequence of small denoising operations is performed using a neural network to obtain back the original image. During each step of the reverse process, we perform a denoising operation to the image  $x_t$  to obtain back  $x_{t-1}$ . For this, a neural network  $f_\theta$  is used to model the parameters of the reverse distribution  $p(x_{t-1}|x_t) := \mathcal{N}(x_{t-1} : \mu_\theta(x_t, t), \Sigma_\theta(x_t, t))$ . The parameters for this network  $\theta$  is obtained by minimizing the KL divergence between the forward and reverse distributions over all timesteps. During optimization, sampling from the distribution  $q(x_t|x_{t-1})$  requires knowledge of  $x_{t-1}$  which requires a sequence of operations to be computed as per equation 2. The marginal distribution of  $x_t$  given  $x_0$  can be derived by marginalizing out the intermediate latent variables as:

$$q(x_t|x_0) = \mathcal{N}(x_t; \sqrt{\gamma_t}x_0, (1 - \gamma_t)\mathbf{I}), \quad (2)$$

where  $\gamma_t = \prod_{i=1}^t \alpha_i$ . Hence simplifying the calculation procedure. Furthermore, Sohl *et al.* [42] has showed minimizing the KL divergence between the forward and reverse distributions could be simplified by using the posterior distribution  $q(x_t|x_{t-1}, x_0)$  instead of the forward distribution  $q(x_t|x_{t-1})$ . Under the Markovian assumptions, Using equations 1 and 2, the posterior distribution can be derived as:

$$q(x_{t-1}|x_t, x_0) = \mathcal{N}(x_{t-1}, \mu, \sigma^2 \mathbf{I}), \quad (3)$$

where

$$\mu(x_t, x_0) = \frac{\sqrt{\gamma_{t-1}}(1 - \alpha_t)}{1 - \gamma_t}x_0 + \frac{\sqrt{\alpha_t}(1 - \gamma_{t-1})}{1 - \gamma_t}x_t \text{ and } \sigma^2 = \frac{(1 - \gamma_{t-1})(1 - \alpha_t)}{1 - \gamma_t}. \quad (4)$$

This posterior distribution is further utilized when parameterizing the reverse Markov chain and formulating a variational lower bound on the log-likelihood of the reverse chain. While optimizing, the covariance matrix for both the distributions  $q(x_{t-1}|x_t, x_0)$  and  $p(x_{t-1}|x_t)$  is usually considered the same and the network  $f_\theta$  predicts the mean of the distribution.

**Optimizing the Diffusion Model.** The denoising model  $f_\theta$  takes as input the noisy image  $x_t$ :

$$x_t = \sqrt{\gamma}x_0 + \sqrt{1-\gamma}\epsilon, \text{ where } \epsilon = \mathcal{N}(\mathbf{0}, \mathbf{I}) \quad (5)$$

and the timestep  $t$  and aims to recover the mean of the posterior distribution. Recent work by Ho *et al.*[20] has simplified this training objective for optimizing the parameters of the network and proposed a simplified objective defined by:

$$\mathbb{E}_{x_0, \epsilon} \|f_\theta(\tilde{x}, t) - \epsilon\|_2^2, \text{ where } \epsilon = \mathcal{N}(\mathbf{0}, \mathbf{I}). \quad (6)$$

**Inference (i.e., sampling).** The inference is defined as the reverse Markovian process which goes in the reverse direction of the forward diffusion process. The inference starts from Gaussian noise  $x_T$ , and  $x_t$  at each timestep  $t$  is iteratively denoised to get back  $x_{t-1}$  according to:

$$x_{t-1} \leftarrow \frac{1}{\sqrt{\alpha_t}} \left( x_t - \frac{1-\alpha_t}{\sqrt{1-\gamma_t}} f_\theta(x_t, t) \right) + \gamma_t z, \text{ where } z = \mathcal{N}(\mathbf{0}, \mathbf{I}), \quad (7)$$

for  $t = T, \dots, 1$ .

## 2.2 Remote sensing CD

Although there exists a wide-variety of classical methods to detect the changes from multi-temporal images such as ImageDiff, ImageRatio [29], ImageRegr [30], CVA [40], DPCA [14], MAD [34], IRMAD [35] and PCDA [15], the current research on remote sensing CD has largely reshaped by deep learning due to its powerful discriminative ability [1]. The existing deep learning based remote sensing CD frameworks are mainly based on convolutional networks (such as FC-EF [13], FC-Siam-conc [13], and FC-Siam-diff [13, 2], and DS-IFN [53], DASNet [9]), *attention modules* (such as ADS-Net [46], and DDCNN [36]), transformer networks (such as BIT [6] and ChangeFormer [3]), or the combination of them (such as [55]). During the early stage of CD research, the backbones of these models (i.e., the feature extractor) are initialized with ImageNet [25] pre-trained weights, due to the limited availability of large-scale aerial scene classification datasets. However, the large domain gap between real and aerial images [47], the emergence of large-scale aerial scene classification datasets (like MillionAID [28], fMoW [12] and BigEarthNet [45]), and the new findings on unsupervised pre-training techniques such as contrastive pre-training [31] motivated and made it possible to pre-train the backbone on aerial images which resulted in faster convergence in the training and significant boost in CD performance than before [47]. However, we see that there is still a quite large room for improvements because current pre-training methods either require aerial scene classification datasets for supervised pre-training (like BigEarthNet [45]) or paired multi-temporal images for self-supervised pre-training (like SeCo [31]), which limits their ability to harness information from millions off-the-shelf unlabeled remote sensing images.

In this study, for the first time, we show that diffusion probabilistic models are extremely useful in overcoming the above limitations in current remote sensing pre-training methods. More specifically, we train a diffusion model on millions of off-the-shelf remote sensing images to learn the key semantics of aerial images, and then use the multi-scale features from the diffusion decoder as the inputs to train a CD classifier under the limited availability of pixel-wise labels.

## 3 Proposed approach for CD

The proposed CD approach consists of two steps: **(1) Training the diffusion model** on a large collection of off-the-shelf remote sensing images to learn the key semantics in aerial images, and **(2) Training a CD classifier** on limited pixel-wise change labels, that takes the deep feature representations from the diffusion decoder as the inputs and outputs the change prediction maps.

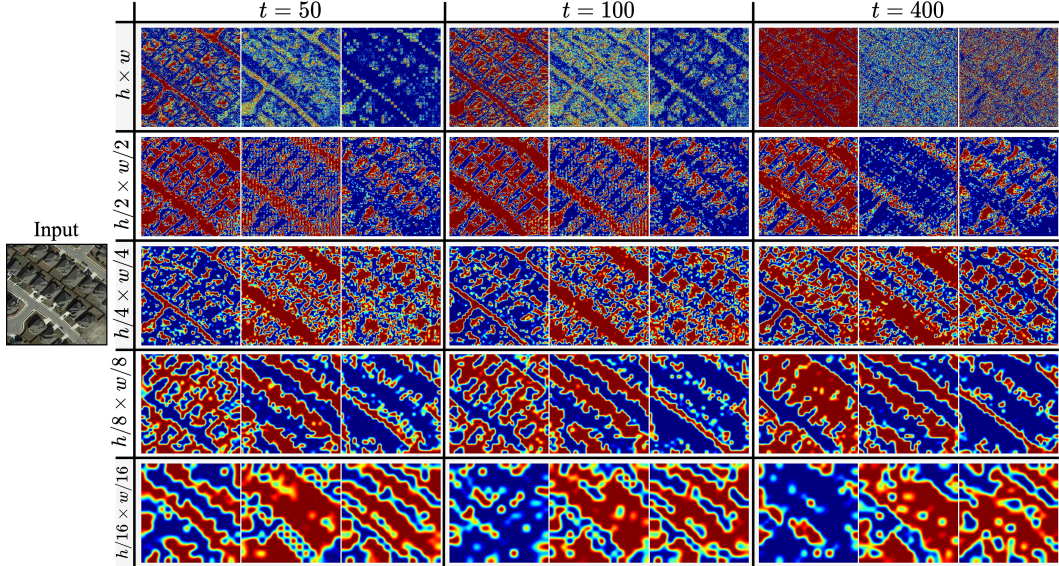


Figure 3: Multi-scale feature representations from the diffusion decoder for different noise levels.

### 3.1 Pre-training the diffusion model on off-the-shelf remote sensing data

In order to train the diffusion model, we first collect a large amount of 3-channel (i.e., RGB) remote sensing images ( $\sim 1M$ ) of Sentinel-2 [16] patches without any human supervision. More specifically, we use Google Earth Engine [19] to process and download imagery patches from around 200K locations around the world [31], where each patch covers an earth resolution of approximately  $2.65 \times 2.65$  km. Next, we train the SOTA unconditional U-Net like [41] diffusion model (see Fig. 1) on the collected dataset until it can generate images closer to real aerial images, as shown in Fig. 1.

### 3.2 Extracting representations of pre-change and post-change images from diffusion model

The pre-trained diffusion model is then utilized to extract the feature representations of pre-change ( $I_a$ ) and post-change ( $I_b$ ) images. Specifically, we first create the noisy version of the given input image following Eqn. (5), and then processes it through the diffusion model to obtain the feature representations (see Fig. 4) of size  $h \times w$ ,  $h/2 \times w/2$ ,  $h/4 \times w/4$ ,  $h/8 \times w/8$ , and  $h/16 \times w/16$ . Figure 3 shows such multi-level feature representation for a given input image for different amount of noise levels added to the input (i.e.,  $t$ ). From the figure, we can see that the diffusion models are also capable of extracting the hierarchical feature representations (i.e., semantics) of the input images, where the features at  $h \times w$  and  $h/2 \times w/2$  scales represents simple patterns like edges and gradients, while features at  $w/4 \times w/4$ ,  $w/8 \times w/8$ , and  $w/16 \times w/16$  scales represent more abstract features. Furthermore, unlike other deep learning architectures, we can also obtain different augmented versions of the feature representations by changing the amount of noise added to the input that can be further utilized to train a robust and generalized CD head under limited pixel-level change labels. In an ablation study, we show that incorporating multi-level features corresponds to different levels of noisy images can significantly improve the CD performance.

### 3.3 Training the lightweight CD network

Next, we train a lightweight CD head that takes multi-scale deep feature representations of pre- and post-change images obtained from the diffusion model as the inputs. Specifically, the network first computes the difference between the multi-level features of pre- and post-change images, and then pass them through a channel-spatial attention module [39], followed by a convolutional classifier to obtain the final change prediction map as depicted in Fig. 4. See the supplementary material for more information on the CD network architecture.

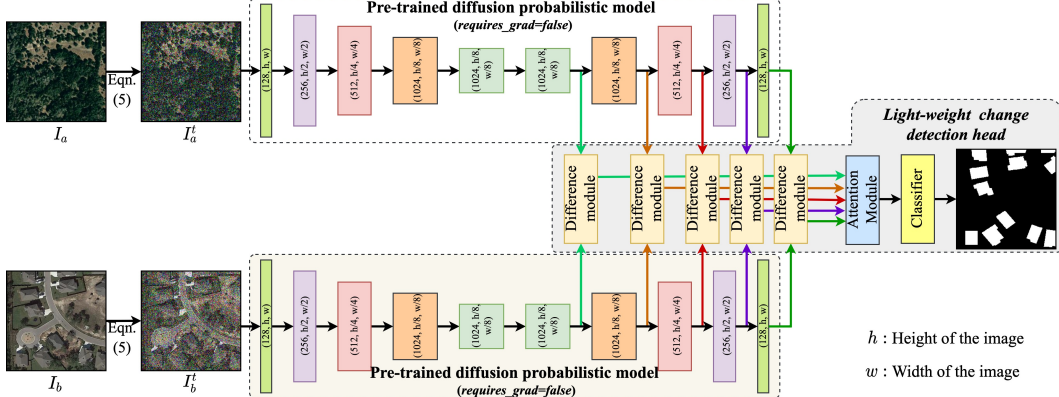


Figure 4: Proposed CD approach. We fine-tune a light-weight CD head which takes multi-level feature representations from the pre-trained diffusion model as inputs and outputs change prediction map.

## 4 Experimental setup

### 4.1 Detests and training Details

**Pre-training the diffusion model:** As we discussed in Sec. 3.1, we train a SOTA unconditional U-Net like diffusion model [41] on off-the-shelf remote sensing images collected from Google Earth Engine without any human supervision. Consistent with [41, 20], we use the Adam optimizer with a linear warmup schedule over 10k training steps, followed by a fixed learning rate of  $1e - 5$ .

**Training CD network:** We perform CD experiments on four publically available CD datasets, namely **LEVIR-CD** [7], **WHU-CD** [21], **DSIFN-CD** [54], and **CDD** [26]. Among these, LEVIR-CD and WHU-CD are building CD datasets, and DSIFN-CD and CDD are general CD datasets. Following the previous works [6, 3], we utilize the patches of size  $256 \times 256$  for training. Given a image, we first extract the multi-level feature representations from the pre-trained diffusion model and feed these features as the inputs to the CD network. We optimize the parameters of CD head with the cross-entropy (CE) loss using the AdamW optimizer, while keeping the parameters of the pre-trained diffusion model freezed. We use the initial learning rate of  $1e - 5$  and linearly decay it to zero over 120 epochs. We optimize the CD head on `val`-set of the datasets and report the results on the `test`-set. We experiment with different sampling locations (i.e.,  $t$ ) in the noise-schedule to find out the optimal feature representations for CD such as  $t = 5, 50, 100, 400$ , and  $650$ , and we discuss how the CD performance varies with  $t$  in the ablation study.

### 4.2 Performance metrics

In order to compare the CD performance of our model with SOTA methods, we report F1 and Intersection over Union (IoU) scores with regard to the change-class as the primary quantitative indices [2, 3, 6]. Additionally, we report overall accuracy (OA) to get a global quality of predictions.

## 5 Results and discussion

In this section, we compare the results of our proposed CD method with several SOTA methods, namely fully-convolutional early-fusion (**FC-EF**) method [13], fully-convolutional siamese-difference (**FC-SD**) method [13], fully-convolutional siamese-concatenation (**FC-SC**) method [13], dual-task constrained siamese network (**DT-SCN**) [27], spatial-temporal attention network (**STA-Net**) [8], densely connected siamese network (**SNU-Net**) [17], bi-temporal image transformer (**BIT**) [6], and transformer-based siamese network (**ChangeFormer**) [3]. Out of these methods, **BIT** and **ChangeFormer** are latest available SOTA methods that use non-local-attention networks (i.e., transformers) for remote sensing CD.

Table 1: The average quantitative results on LEVIR-CD, WHU-CD, DSIFN-CD, and CDD datasets\*.

Method	LEVIR-CD [7]			WHU-CD [21]			DSIFN-CD [54]			CDD [26]		
	F1	IoU	OA	F1	IoU	OA	F1	IoU	OA	F1	IoU	OA
FC-EF [13]	83.40	71.53	98.39	76.73	62.24	98.31	72.17	56.45	83.37	66.93	50.30	93.28
FC-SD [13]	86.31	75.92	98.67	78.95	65.23	98.48	70.55	54.49	84.13	70.61	54.57	94.33
FC-SC [13]	83.69	71.96	98.49	79.85	66.46	98.50	59.71	42.56	87.57	75.11	60.14	94.95
DT-SCN [27]	87.67	78.05	98.77	<b>91.43</b>	<b>84.21</b>	<b>99.35</b>	70.58	54.53	82.87	<b>92.09</b>	<b>85.34</b>	<b>98.16</b>
STANet [8]	87.26	77.40	98.66	82.32	69.95	98.52	64.56	47.66	88.49	84.12	72.22	96.13
IFNet [53]	88.13	78.77	98.87	83.40	71.52	98.83	60.10	42.96	87.83	84.00	71.91	96.03
SNUNet [17]	88.16	78.83	98.82	83.50	71.67	98.71	66.18	49.45	87.34	83.89	72.11	96.23
BIT [6]	<b>89.31</b>	<b>80.68</b>	<b>98.92</b>	<b>90.53</b>	<b>83.39</b>	<b>99.34</b>	<b>87.61</b>	<b>77.96</b>	<b>92.30</b>	88.90	80.01	97.47
ChangeFormer [3]	<b>90.40</b>	<b>82.48</b>	<b>99.04</b>	88.57	79.49	99.12	<b>94.67</b>	<b>88.71</b>	<b>93.23</b>	<b>94.63</b>	<b>89.80</b>	<b>98.74</b>
ddpm-CD	<b>90.91</b>	<b>83.35</b>	<b>99.09</b>	<b>92.65</b>	<b>86.31</b>	<b>99.42</b>	<b>96.65</b>	<b>91.28</b>	<b>97.09</b>	<b>95.62</b>	<b>91.62</b>	<b>98.98</b>

\*All the values are in %. Higher values of CF1, IoU, and OA indicate good CD performance. Color convention: **best**, **2nd-best**, and **3rd-best**.

## 5.1 Quantitative CD Results

Table 1 compares the CD performance of the proposed method with SOTA methods in terms of F1, IoU, and OA scores. We can see that the proposed method outperforms existing SOTA methods by a significant margin on all metrics across all four datasets, empirically validating that diffusion models can extract key semantics that will be useful for CD.

## 5.2 Qualitative CD Results

In addition to the quantitative results, we also visualize some qualitative examples to further highlight the effectiveness of the proposed method over the SOTA methods in Fig. 6, 8, 10 and 12 for LEVIR-CD, WHU-CD, DSIFN-CD and CDD datasets, respectively. From the visual results also we can clearly see that the proposed method is able to detect much complex changes accurately than the existing methods, further demonstrating diffusion model’s ability to extract key semantics from the images.

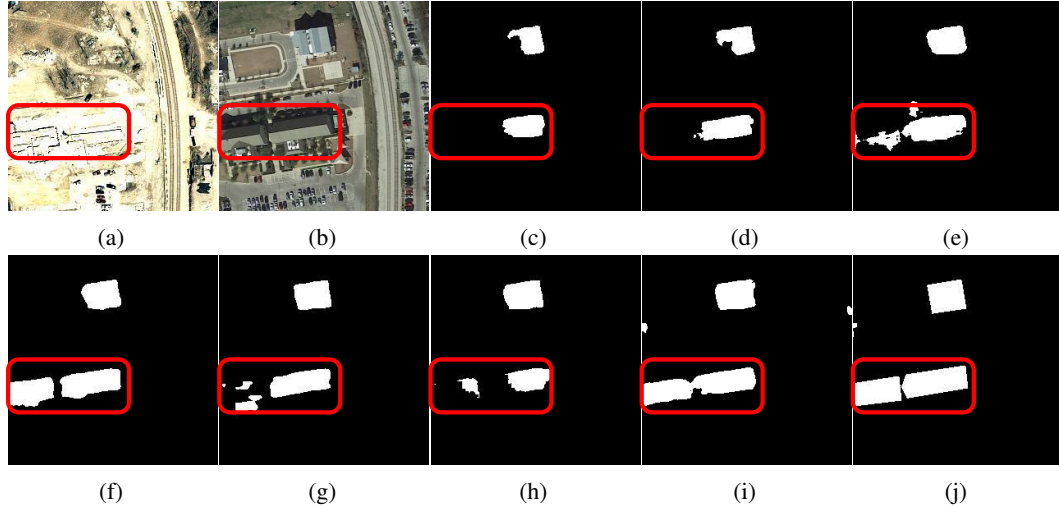


Figure 6: Comparision of different SOTA CD methods on **LEVIR-CD dataset**: (a) Pre-change image, (b) Post-change image, (c) FC-EF, (d) FC-Siam-Di, (e) FC-Siam-Conc, (f) DTCDSCN, (g) BIT, (h) ChangeFormer, (i) ddpm-CD (ours), and (j) Ground-truth.

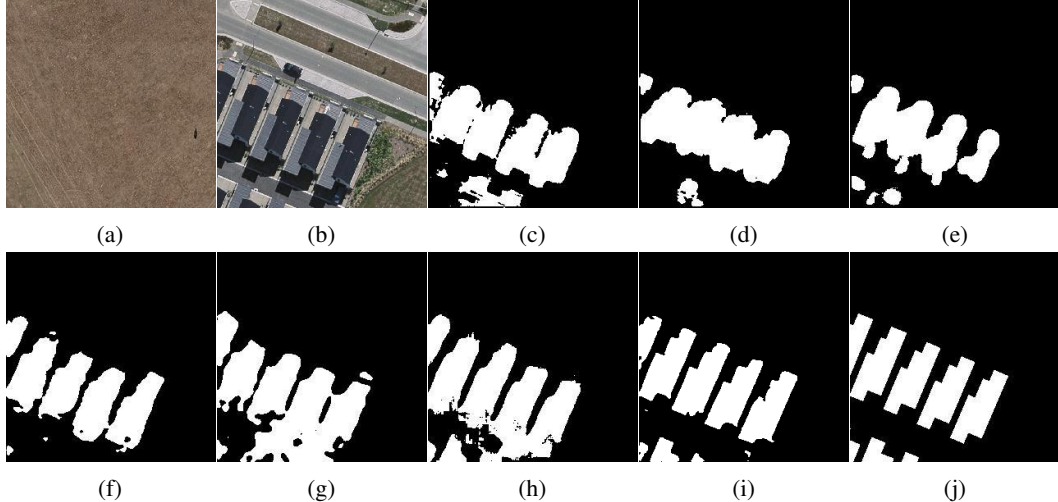


Figure 8: Comparision of different SOTA CD methods on **WHU-CD dataset**: (a) Pre-change image, (b) Post-change image, (c) FC-EF, (d) FC-Siam-Di, (e) FC-Siam-Conc, (f) DTCDSNC, (g) BIT, (h) ChangeFormer, (i) ddpm-CD (ours), and (j) Ground-truth.

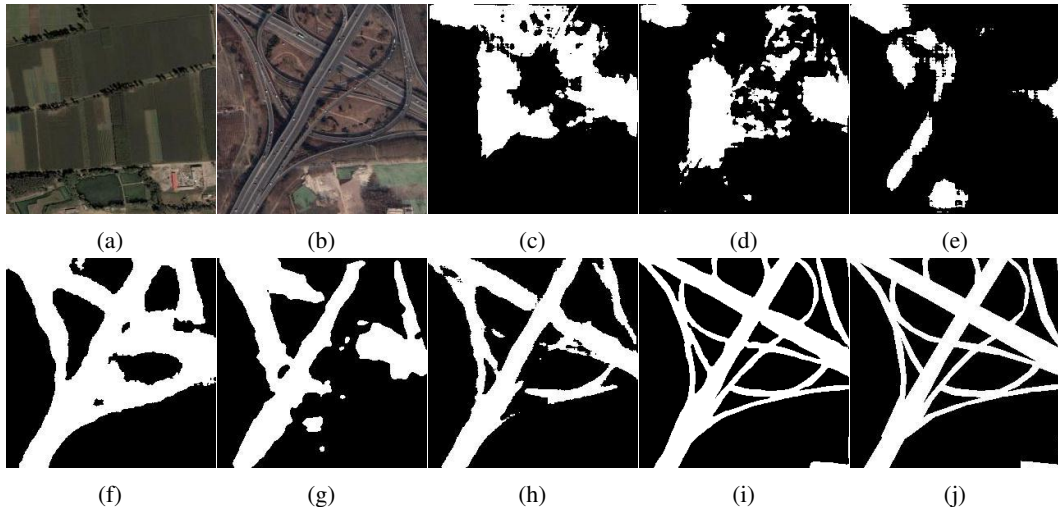


Figure 10: Comparison of different SOTA CD methods on **DSIFN-CD dataset**: (a) Pre-change image, (b) Post-change image, (c) FC-EF, (d) FC-Siam-Di, (e) FC-Siam-Conc, (f) DTCDSNC, (g) BIT, (h) ChangeFormer, (i) ddpm-CD (ours), and (j) Ground-truth.

## 6 Ablation study

In this ablation study, we discuss how the CD performance varies with time-step  $t \in [0, T]$  that we used to extract the feature representation from the diffusion model. To this end, we train the CD classifiers with features sampled from different time-steps  $t$  of the diffusion model to find out best time-step range that provide best semantics required for the CD task. Table 2 shows how the CD performance varies with the features obtained at  $t = 5, 50, 100, (50 \text{ and } 100), (50, 100 \text{ and } 400)$  and  $(50, 100, \text{ and } 650)$  used as inputs to train the CD classifier. We observed the best CD performance across all the datasets when we utilize the feature representations sampled from the range  $t \in [100, 400]$ . Furthermore, we have noticed that, concatenating feature representations of multiple time samples such as  $t = 50, 100$  and  $400$  results in further improvement in CD. Therefore, our final CD classifier takes feature representations sampled at  $t = 50, 100$ , and  $400$  as inputs.

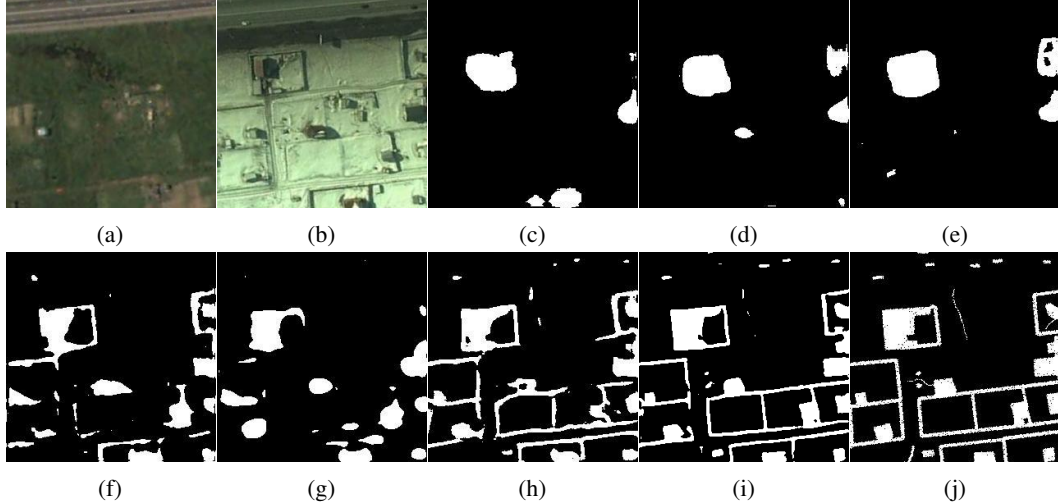


Figure 12: Comparison of different SOTA CD methods on **CDD dataset**: (a) Pre-change image, (b) Post-change image, (c) FC-EF, (d) FC-Siam-Di, (e) FC-Siam-Conc, (f) DTCDSNC, (g) BIT, (h) ChangeFormer, (i) ddpm-CD (ours), and (j) Ground-truth.

Table 2: How the CD performance varies with the time step  $t$  that we used to extract features from the diffusion model on val-set of LEVIR-CD, WHU-CD, DSIFN-CD, and CDD datasets.

Time step $t$	LEVIR-CD [7]			WHU-CD [21]			DSIFN-CD [54]			CDD [26]		
	F1	IoU	OA	F1	IoU	OA	F1	IoU	OA	F1	IoU	OA
5	89.71	81.35	99.15	91.57	84.46	99.19	93.87	88.39	96.09	91.24	83.89	91.24
50	90.66	82.90	99.23	92.74	86.47	99.31	94.17	88.99	96.29	93.78	88.28	98.60
100	90.50	82.65	99.21	92.78	86.54	99.31	94.95	90.39	96.77	94.32	89.25	98.72
150	90.08	81.95	99.18	92.34	85.77	99.27	94.59	89.74	96.54	94.34	89.29	98.75
50, 100	<b>91.02</b>	<b>83.52</b>	<b>99.26</b>	<b>93.09</b>	<b>87.07</b>	<b>99.34</b>	<b>94.51</b>	<b>89.61</b>	<b>96.51</b>	<b>94.91</b>	<b>90.31</b>	<b>98.85</b>
50, 100, 400	<b>91.26</b>	<b>83.92</b>	<b>99.28</b>	<b>93.50</b>	<b>87.80</b>	<b>99.38</b>	<b>95.38</b>	<b>91.18</b>	<b>97.05</b>	<b>95.64</b>	<b>91.64</b>	<b>99.00</b>
50, 100, 650	<b>91.10</b>	<b>83.67</b>	<b>99.26</b>	<b>93.02</b>	<b>86.95</b>	<b>99.33</b>	<b>95.07</b>	<b>90.62</b>	<b>96.87</b>	<b>95.24</b>	<b>90.90</b>	<b>98.92</b>

\*All the values are in %. Higher values of F1, IoU, and OA indicate good CD performance. Color convention: **best**, **2nd-best**, and **3rd-best**.

## 7 Conclusion

In this paper, we proposed a novel remote sensing CD method based on denoising diffusion probabilistic models. The proposed method first pre-train an unconditional denoising diffusion probabilistic model on millions of off-the-shelf remote sensing images available to the public to learn the key semantics in the remote sensing images. The pre-trained diffusion model is then utilized to extract multi-scale feature representations from a given satellite image to train a light-weight CD classifier. The proposed method differs from existing deep CD methods mainly in two aspects: (1) The training of diffusion probabilistic model which serves as the feature extractor in our case does not require any type of labeled data which is indeed valuable specially for remote sensing applications due to the fact that most of the publicly available millions of remote sensing data are unlabeled or difficult to annotate. (2) Unlike existing deep CD algorithms we keep the weights of the trained diffusion model freezed and only optimize the parameters of lightweight CD classifier, that helps efficient and fast deployment on new CD applications or datasets. Above all these advantages of the proposed approach, it also achieves significantly better performance compared to SOTA CD methods making it as the new SOTA method for remote sensing CD.

## References

[1] Anju Asokan and J Anitha. Change detection techniques for remote sensing applications: a survey. *Earth Science Informatics*, 12(2):143–160, 2019.

- [2] Wele Gedara Chaminda Bandara and Vishal M Patel. Revisiting consistency regularization for semi-supervised change detection in remote sensing images. *arXiv preprint arXiv:2204.08454*, 2022.
- [3] Wele Gedara Chaminda Bandara and Vishal M Patel. A transformer-based siamese network for change detection. *arXiv preprint arXiv:2201.01293*, 2022.
- [4] Dmitry Baranchuk, Ivan Rubachev, Andrey Voynov, Valentin Khrulkov, and Artem Babenko. Label-efficient semantic segmentation with diffusion models. *arXiv preprint arXiv:2112.03126*, 2021.
- [5] Stephan Bojinski, Michel Verstraete, Thomas C Peterson, Carolin Richter, Adrian Simmons, and Michael Zemp. The concept of essential climate variables in support of climate research, applications, and policy. *Bulletin of the American Meteorological Society*, 95(9):1431–1443, 2014.
- [6] Hao Chen, Zipeng Qi, and Zhenwei Shi. Remote sensing image change detection with transformers. *IEEE Transactions on Geoscience and Remote Sensing*, 2021.
- [7] Hao Chen and Zhenwei Shi. A spatial-temporal attention-based method and a new dataset for remote sensing image change detection. *Remote Sensing*, 12(10):1662, 2020.
- [8] Hao Chen and Zhenwei Shi. A spatial-temporal attention-based method and a new dataset for remote sensing image change detection. *Remote Sensing*, 12(10):1662, 2020.
- [9] Jie Chen, Ziyang Yuan, Jian Peng, Li Chen, Haozhe Huang, Jiawei Zhu, Yu Liu, and Haifeng Li. Dasnet: Dual attentive fully convolutional siamese networks for change detection in high-resolution satellite images. *IEEE Journal of Selected Topics in Applied Earth Observations and Remote Sensing*, 14:1194–1206, 2021.
- [10] Ting Chen, Simon Kornblith, Mohammad Norouzi, and Geoffrey Hinton. A simple framework for contrastive learning of visual representations. In *International conference on machine learning*, pages 1597–1607. PMLR, 2020.
- [11] Xinlei Chen, Haoqi Fan, Ross Girshick, and Kaiming He. Improved baselines with momentum contrastive learning. *arXiv preprint arXiv:2003.04297*, 2020.
- [12] Gordon Christie, Neil Fendley, James Wilson, and Ryan Mukherjee. Functional map of the world. In *Proceedings of the IEEE Conference on Computer Vision and Pattern Recognition*, pages 6172–6180, 2018.
- [13] Rodrigo Caye Daudt, Bertr Le Saux, and Alexandre Boulch. Fully convolutional siamese networks for change detection. In *2018 25th IEEE International Conference on Image Processing (ICIP)*, pages 4063–4067. IEEE, 2018.
- [14] JS Deng, K Wang, YH Deng, and GJ Qi. Pca-based land-use change detection and analysis using multitemporal and multisensor satellite data. *International Journal of Remote Sensing*, 29(16):4823–4838, 2008.
- [15] M Dharani and G Sreenivasulu. Land use and land cover change detection by using principal component analysis and morphological operations in remote sensing applications. *International Journal of Computers and Applications*, 43(5):462–471, 2021.
- [16] Matthias Drusch, Umberto Del Bello, Sébastien Carlier, Olivier Colin, Veronica Fernandez, Ferran Gascon, Bianca Hoersch, Claudia Isola, Paolo Laberinti, Philippe Martimort, et al. Sentinel-2: Esa’s optical high-resolution mission for gmes operational services. *Remote sensing of Environment*, 120:25–36, 2012.
- [17] Sheng Fang, Kaiyu Li, Jinyuan Shao, and Zhe Li. Snunet-cd: A densely connected siamese network for change detection of vhr images. *IEEE Geoscience and Remote Sensing Letters*, 19:1–5, 2021.
- [18] Ian Goodfellow, Jean Pouget-Abadie, Mehdi Mirza, Bing Xu, David Warde-Farley, Sherjil Ozair, Aaron Courville, and Yoshua Bengio. Generative adversarial nets. *Advances in neural information processing systems*, 27, 2014.
- [19] Noel Gorelick, Matt Hancher, Mike Dixon, Simon Ilyushchenko, David Thau, and Rebecca Moore. Google earth engine: Planetary-scale geospatial analysis for everyone. *Remote sensing of Environment*, 202:18–27, 2017.
- [20] Jonathan Ho, Ajay Jain, and Pieter Abbeel. Denoising diffusion probabilistic models. *Advances in Neural Information Processing Systems*, 33:6840–6851, 2020.
- [21] Shunping Ji, Shiqing Wei, and Meng Lu. Fully convolutional networks for multisource building extraction from an open aerial and satellite imagery data set. *IEEE Transactions on Geoscience and Remote Sensing*, 57(1):574–586, 2018.
- [22] Peng Jiang, Fanglin Gu, Yunhai Wang, Changhe Tu, and Baoquan Chen. Difnet: Semantic segmentation by diffusion networks. *Advances in Neural Information Processing Systems*, 31, 2018.
- [23] Diederik P Kingma and Max Welling. Auto-encoding variational bayes. *arXiv preprint arXiv:1312.6114*, 2013.
- [24] Diederik P Kingma and Max Welling. An introduction to variational autoencoders. *arXiv preprint arXiv:1906.02691*, 2019.

[25] Alex Krizhevsky, Ilya Sutskever, and Geoffrey E Hinton. Imagenet classification with deep convolutional neural networks. *Advances in neural information processing systems*, 25, 2012.

[26] MA Lebedev, Yu V Vizilter, OV Vygolov, VA Knyaz, and A Yu Rubis. Change detection in remote sensing images using conditional adversarial networks. *International Archives of the Photogrammetry, Remote Sensing & Spatial Information Sciences*, 42(2), 2018.

[27] Yi Liu, Chao Pang, Zongqian Zhan, Xiaomeng Zhang, and Xue Yang. Building change detection for remote sensing images using a dual-task constrained deep siamese convolutional network model. *IEEE Geoscience and Remote Sensing Letters*, 18(5):811–815, 2020.

[28] Yang Long, Gui-Song Xia, Shengyang Li, Wen Yang, Michael Ying Yang, Xiao Xiang Zhu, Liangpei Zhang, and Deren Li. On creating benchmark dataset for aerial image interpretation: Reviews, guidances, and million-aid. *IEEE Journal of Selected Topics in Applied Earth Observations and Remote Sensing*, 14:4205–4230, 2021.

[29] Dengsheng Lu, Paul Mausel, Eduardo Brondizio, and Emilio Moran. Change detection techniques. *International journal of remote sensing*, 25(12):2365–2401, 2004.

[30] Luigi Tommaso Luppino, Filippo Maria Bianchi, Gabriele Moser, and Stian Normann Anfinsen. Unsupervised image regression for heterogeneous change detection. *IEEE Transactions on Geoscience and Remote Sensing*, 57(12):9960–9975, 2019.

[31] Oscar Mañas, Alexandre Lacoste, Xavier Giro-i Nieto, David Vazquez, and Pau Rodriguez. Seasonal contrast: Unsupervised pre-training from uncurated remote sensing data. In *Proceedings of the IEEE/CVF International Conference on Computer Vision*, pages 9414–9423, 2021.

[32] Nithin Gopalakrishnan Nair, Wele Gedara Chaminda Bandara, and Vishal M Patel. Image generation with multimodal priors using denoising diffusion probabilistic models. *arXiv preprint arXiv:2206.05039*, 2022.

[33] Alexander Quinn Nichol and Prafulla Dhariwal. Improved denoising diffusion probabilistic models. In *International Conference on Machine Learning*, pages 8162–8171. PMLR, 2021.

[34] Allan A Nielsen, Knut Conradsen, and James J Simpson. Multivariate alteration detection (mad) and maf postprocessing in multispectral, bitemporal image data: New approaches to change detection studies. *Remote Sensing of Environment*, 64(1):1–19, 1998.

[35] Allan Aasbjerg Nielsen. The regularized iteratively reweighted mad method for change detection in multi-and hyperspectral data. *IEEE Transactions on Image processing*, 16(2):463–478, 2007.

[36] Xueli Peng, Ruofei Zhong, Zhen Li, and Qingyang Li. Optical remote sensing image change detection based on attention mechanism and image difference. *IEEE Transactions on Geoscience and Remote Sensing*, 59(9):7296–7307, 2021.

[37] Malsha V Perera, Nithin Gopalakrishnan Nair, Wele Gedara Chaminda Bandara, and Vishal M Patel. Sar despeckling using a denoising diffusion probabilistic model. *arXiv preprint arXiv:2206.04514*, 2022.

[38] Robin Rombach, Andreas Blattmann, Dominik Lorenz, Patrick Esser, and Björn Ommer. High-resolution image synthesis with latent diffusion models. *arXiv preprint arXiv:2112.10752*, 2021.

[39] Abhijit Guha Roy, Nassir Navab, and Christian Wachinger. Concurrent spatial and channel ‘squeeze & excitation’ in fully convolutional networks. In *International conference on medical image computing and computer-assisted intervention*, pages 421–429. Springer, 2018.

[40] Sudipan Saha, Francesca Bovolo, and Lorenzo Bruzzone. Unsupervised deep change vector analysis for multiple-change detection in vhr images. *IEEE Transactions on Geoscience and Remote Sensing*, 57(6):3677–3693, 2019.

[41] Chitwan Saharia, Jonathan Ho, William Chan, Tim Salimans, David J Fleet, and Mohammad Norouzi. Image super-resolution via iterative refinement. *arXiv preprint arXiv:2104.07636*, 2021.

[42] Jascha Sohl-Dickstein, Eric Weiss, Niru Maheswaranathan, and Surya Ganguli. Deep unsupervised learning using nonequilibrium thermodynamics. In *International Conference on Machine Learning*, pages 2256–2265. PMLR, 2015.

[43] Yang Song, Jascha Sohl-Dickstein, Diederik P Kingma, Abhishek Kumar, Stefano Ermon, and Ben Poole. Score-based generative modeling through stochastic differential equations. *arXiv preprint arXiv:2011.13456*, 2020.

[44] Nasim Souly, Concetto Spampinato, and Mubarak Shah. Semi and weakly supervised semantic segmentation using generative adversarial network. *arXiv preprint arXiv:1703.09695*, 2017.

[45] Gencer Sumbul, Marcela Charfuelan, Begüm Demir, and Volker Markl. Bigearthnet: A large-scale benchmark archive for remote sensing image understanding. In *IGARSS 2019-2019 IEEE International Geoscience and Remote Sensing Symposium*, pages 5901–5904. IEEE, 2019.

- [46] Decheng Wang, Xiangning Chen, Mingyong Jiang, Shuhan Du, Bijie Xu, and Junda Wang. Ads-net:an attention-based deeply supervised network for remote sensing image change detection. *International Journal of Applied Earth Observation and Geoinformation*, 101:102348, 2021.
- [47] Di Wang, Jing Zhang, Bo Du, Gui-Song Xia, and Dacheng Tao. An empirical study of remote sensing pretraining. *arXiv preprint arXiv:2204.02825*, 2022.
- [48] Junjue Wang, Zhuo Zheng, Ma Ailong, Xiaoyan Lu, and Yanfei Zhong. LoveDA: A remote sensing land-cover dataset for domain adaptive semantic segmentation. In *Thirty-fifth Conference on Neural Information Processing Systems Datasets and Benchmarks Track (Round 2)*, 2021.
- [49] Dawei Wen, Xin Huang, Francesca Bovolo, Jiaji Li, Xinli Ke, Anlu Zhang, and Jon Atli Benediktsson. Change detection from very-high-spatial-resolution optical remote sensing images: Methods, applications, and future directions. *IEEE Geoscience and Remote Sensing Magazine*, 9(4):68–101, 2021.
- [50] Jay Whang, Mauricio Delbracio, Hossein Talebi, Chitwan Saharia, Alexandros G Dimakis, and Peyman Milanfar. Deblurring via stochastic refinement. *arXiv preprint arXiv:2112.02475*, 2021.
- [51] Julia Wolleb, Robin Sandkühler, Florentin Bieder, Philippe Valmaggia, and Philippe C Cattin. Diffusion models for implicit image segmentation ensembles. *arXiv preprint arXiv:2112.03145*, 2021.
- [52] Yufei Xu, Qiming Zhang, Jing Zhang, and Dacheng Tao. Regioncl: Can simple region swapping contribute to contrastive learning? *arXiv preprint arXiv:2111.12309*, 2021.
- [53] Chenxiao Zhang, Peng Yue, Deodato Tapete, Liangcun Jiang, Boyi Shangguan, Li Huang, and Guangchao Liu. A deeply supervised image fusion network for change detection in high resolution bi-temporal remote sensing images. *ISPRS Journal of Photogrammetry and Remote Sensing*, 166:183–200, 2020.
- [54] Chenxiao Zhang, Peng Yue, Deodato Tapete, Liangcun Jiang, Boyi Shangguan, Li Huang, and Guangchao Liu. A deeply supervised image fusion network for change detection in high resolution bi-temporal remote sensing images. *ISPRS Journal of Photogrammetry and Remote Sensing*, 166:183–200, 2020.
- [55] Cui Zhang, Liejun Wang, Shuli Cheng, and Yongming Li. Swinsunet: Pure transformer network for remote sensing image change detection. *IEEE Transactions on Geoscience and Remote Sensing*, 60:1–13, 2022.

## 8 Additional qualitative results

### 8.1 LEVIR-CD dataset

Figure 13, 14, 15, and 16 show additional qualitative results on LEVIR-CD dataset.

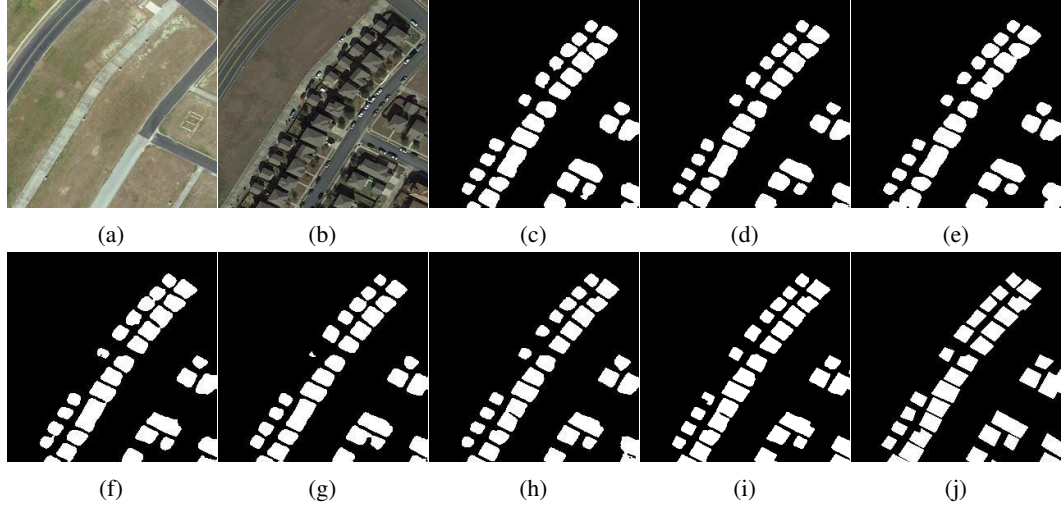


Figure 13: Comparison of different state-of-the-art CD methods on **LEVIR-CD dataset**: (a) Pre-change image, (b) Post-change image, (c) FC-EF [13], (d) FC-Siam-Di [13], (e) FC-Siam-Conc [13], (f) DT-SCN [27], (g) BIT [6], (h) ChangeFormer [3], (i) ddpm-CD (*ours*), and (j) Ground-truth.

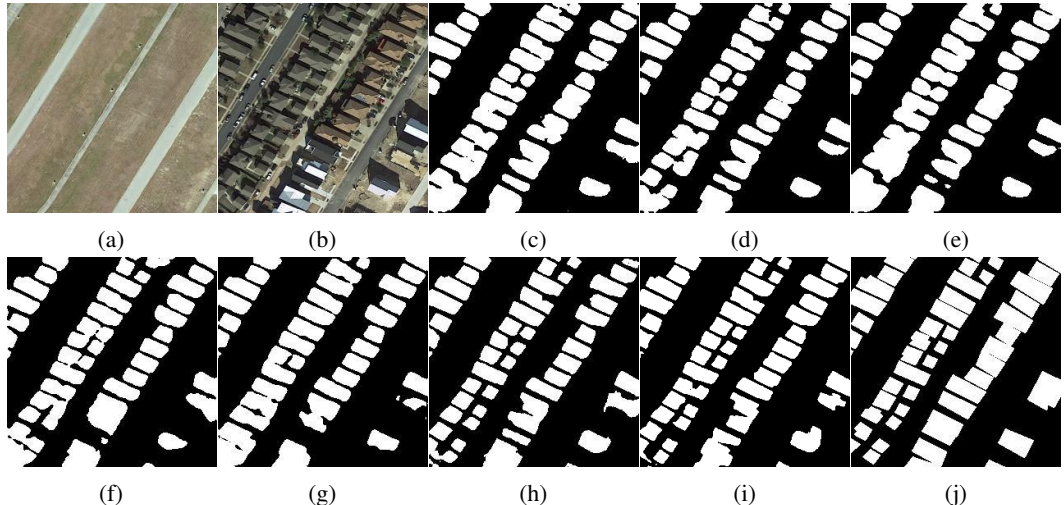


Figure 14: Comparison of different state-of-the-art CD methods on **LEVIR-CD dataset**: (a) Pre-change image, (b) Post-change image, (c) FC-EF [13], (d) FC-Siam-Di [13], (e) FC-Siam-Conc [13], (f) DT-SCN [27], (g) BIT [6], (h) ChangeFormer [3], (i) ddpm-CD (*ours*), and (j) Ground-truth.

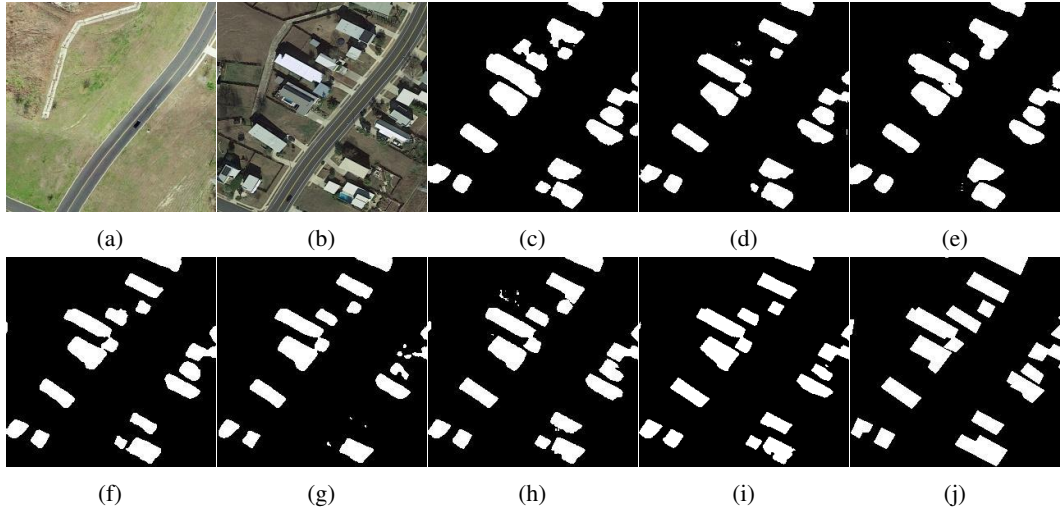


Figure 15: Comparision of different state-of-the-art CD methods on **LEVIR-CD dataset**: (a) Pre-change image, (b) Post-change image, (c) FC-EF [13], (d) FC-Siam-Di [13], (e) FC-Siam-Conc [13], (f) DT-SCN [27], (g) BIT [6], (h) ChangeFormer [3], (i) ddpm-CD (*ours*), and (j) Ground-truth.

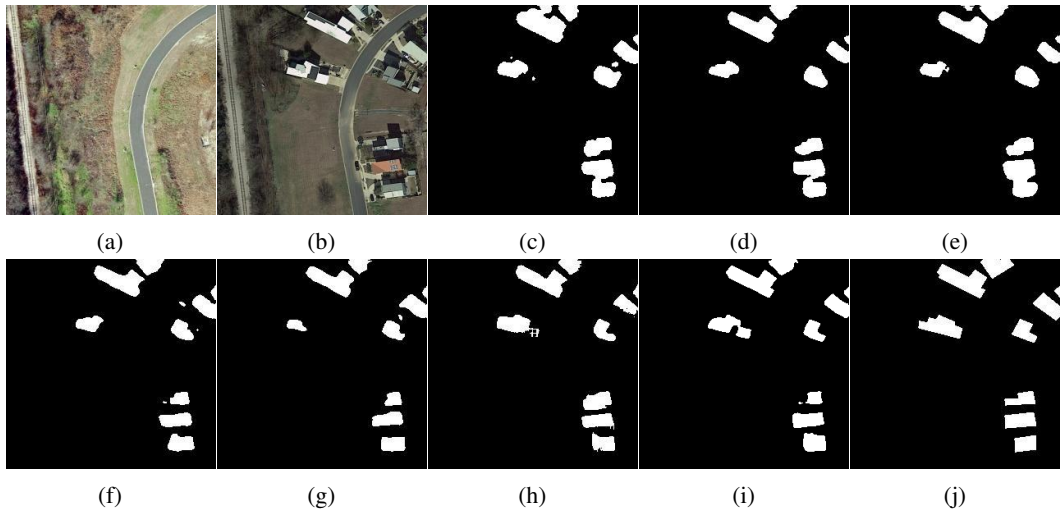


Figure 16: Comparision of different state-of-the-art CD methods on **LEVIR-CD dataset**: (a) Pre-change image, (b) Post-change image, (c) FC-EF [13], (d) FC-Siam-Di [13], (e) FC-Siam-Conc [13], (f) DT-SCN [27], (g) BIT [6], (h) ChangeFormer [3], (i) ddpm-CD (*ours*), and (j) Ground-truth.

## 8.2 WHU-CD dataset

Figure 17, 18, 19, 20 and 21 show additional qualitative results on WHU-CD dataset.

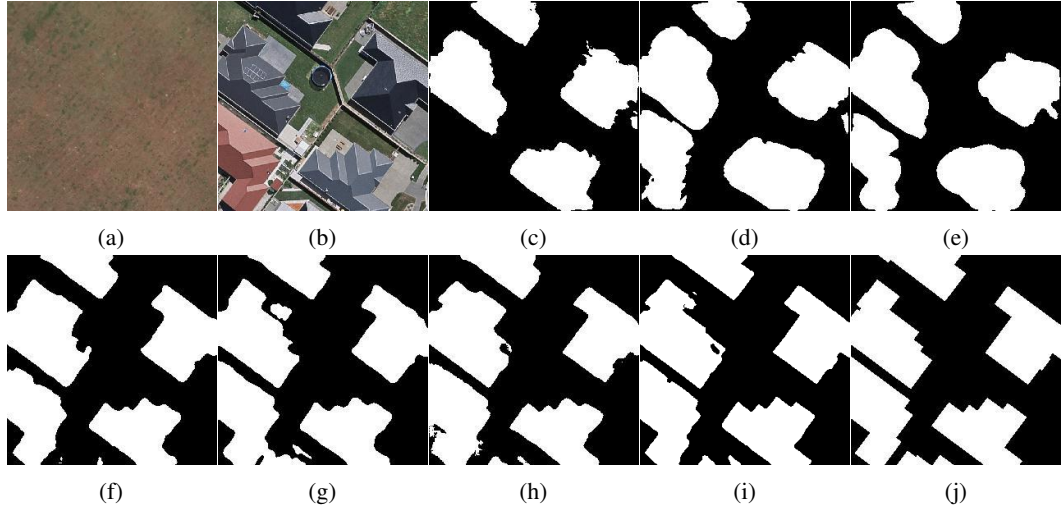


Figure 17: Comparision of different state-of-the-art CD methods on **WHU-CD dataset**: (a) Pre-change image, (b) Post-change image, (c) FC-EF [13], (d) FC-Siam-Di [13], (e) FC-Siam-Conc [13], (f) DT-SCN [27], (g) BIT [6], (h) ChangeFormer [3], (i) ddpm-CD (*ours*), and (j) Ground-truth.

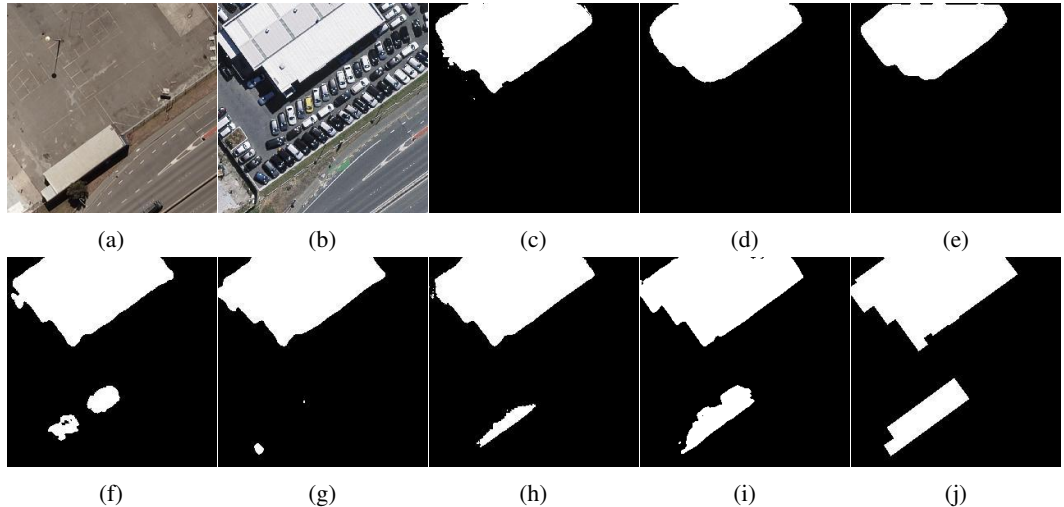


Figure 18: Comparision of different state-of-the-art CD methods on **WHU-CD dataset**: (a) Pre-change image, (b) Post-change image, (c) FC-EF [13], (d) FC-Siam-Di [13], (e) FC-Siam-Conc [13], (f) DT-SCN [27], (g) BIT [6], (h) ChangeFormer [3], (i) ddpm-CD (*ours*), and (j) Ground-truth.

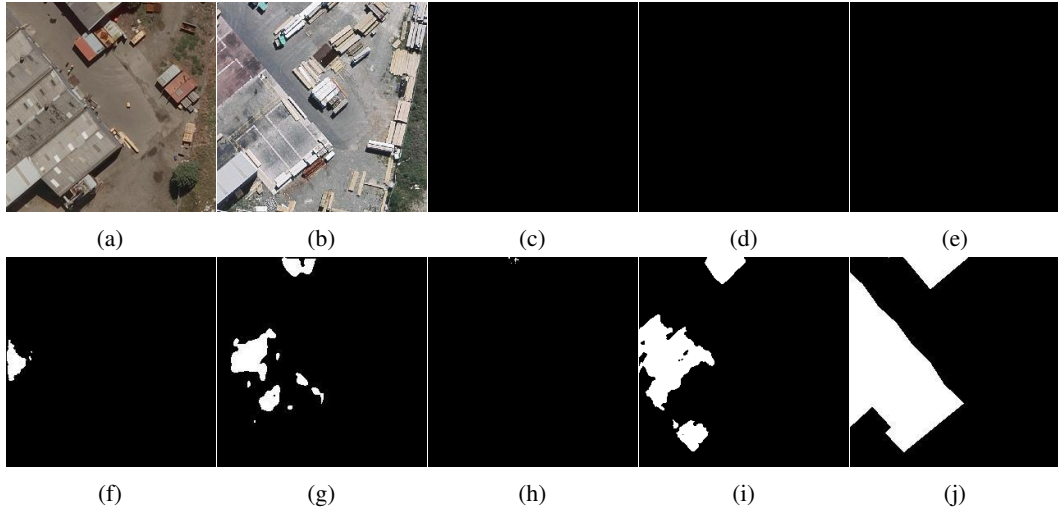


Figure 19: Comparision of different state-of-the-art CD methods on **WHU-CD dataset**: (a) Pre-change image, (b) Post-change image, (c) FC-EF [13], (d) FC-Siam-Di [13], (e) FC-Siam-Conc [13], (f) DT-SCN [27], (g) BIT [6], (h) ChangeFormer [3], (i) ddpm-CD (*ours*), and (j) Ground-truth.

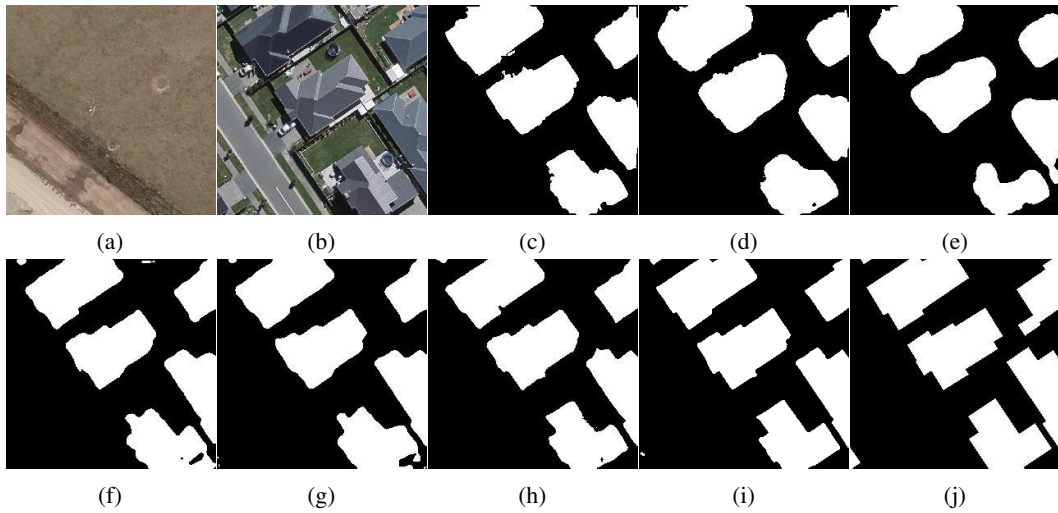


Figure 20: Comparision of different state-of-the-art CD methods on **WHU-CD dataset**: (a) Pre-change image, (b) Post-change image, (c) FC-EF [13], (d) FC-Siam-Di [13], (e) FC-Siam-Conc [13], (f) DT-SCN [27], (g) BIT [6], (h) ChangeFormer [3], (i) ddpm-CD (*ours*), and (j) Ground-truth.

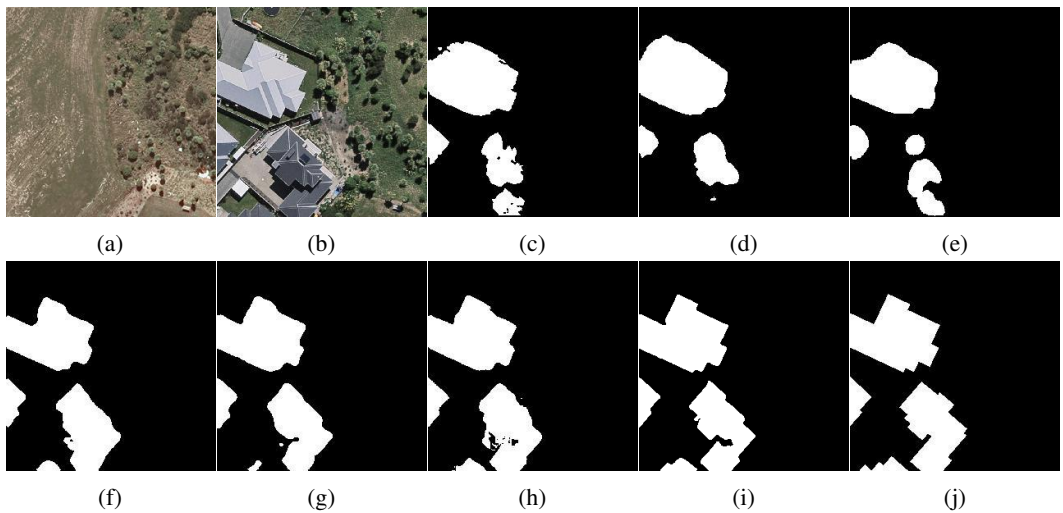


Figure 21: Comparision of different state-of-the-art CD methods on **WHU-CD dataset**: (a) Pre-change image, (b) Post-change image, (c) FC-EF [13], (d) FC-Siam-Di [13], (e) FC-Siam-Conc [13], (f) DT-SCN [27], (g) BIT [6], (h) ChangeFormer [3], (i) ddpm-CD (*ours*), and (j) Ground-truth.